Analysis of Activity States of Local Neuronal Microcircuits in Mouse Brain

Di Jin[1], Boriana Boiadjieva[2], Hendrik Backhaus[3], Michael Fauß[1], Ting Fu[3], Albrecht Stroh[3], Anja Klein[2], and Abdelhak M. Zoubir[1]

[1]*Signal Processing Group* [2]*Communications Engineering Lab*
Technische Universität Darmstadt, Darmstadt, Germany
{jin, fauss, zoubir}@spg.tu-darmstadt.de {b.boiadjieva, a.klein}@nt.tu-darmstadt.de

[3]*Institute for Microscopic Anatomy and Neurobiology*
Johannes Gutenberg-University Mainz, Mainz, Germany
{hendrik.backhaus, ting.fu, albrecht.stroh}@unimedizin-mainz.de

***Abstract*—Time series of neuronal activity corresponding to different activity states in mouse brain are analyzed in the time domain and the time-frequency domain. The signals are associated with either a slow wave brain state or a persistent brain state. For both states, characteristic spectral features are identified and a simple detector is proposed that is able to identify the brain state with low latency and high accuracy. In practice, being able to monitor the brain state online and in real time is crucial for improved *in vivo* experiments and, ultimately, for a causal understanding of brain dynamics.**

***Index Terms*—Brain state, neuronal circuits, detection, hypothesis testing, time-frequency analysis**

I. Introduction

Spontaneous changes of neuronal network activity states are of great interest in neuroscience research [1], [2]. The two brain states investigated in this paper are referred to as the *slow wave* brain state and the *persistent* brain state. The slow wave activity state is characterized by frequent transitions between hyperpolarized Down states and depolarized Up states. It can occur, for example, during *non-rapid-eye-movement sleep* and during many forms of anesthesia, both spontaneously and evoked by brief sensory stimulation [3], [4], [5]. The persistent brain state, in contrast, is characterized by desynchronized neuronal behavior and occurs during *rapid-eye-movement sleep* and active wakefulness [1].

For the experimenter, it is highly attractive to be able to detect these two states with low latency in order to manipulate the experiment in real-time. For instance, depending on the detection result, an experimenter can control the doses of anesthesia drugs to maintain a certain brain state. Therefore, the aim of this paper is to tackle this problem from a signal processing point of view. Its contribution is twofold: first, a detailed discussion of the characteristics of the microcircuit activity in both states in the time and time-frequency domain is given. Here, the focus is on the time-frequency domain, since it admits several distinct features that, to the best of the authors' knowledge, have not been studied in existing work yet. Second, the brain state detection problem is formulated as a binary hypothesis test and a detector is proposed to distinguish between the two states without human intervention. Since the available data is scarce and its interpretation is, to an extent, still the subject of ongoing research, the detector is deliberately kept simple and merely serves as a proof of concept.

The presented results are based on experiments that were conducted on three different mice. Four weeks prior to the experiments, a small craniotomy was performed with a dental drill (Ultimate XL-F, NSK, Trier Germany, and VS1/4HP/005, Meisinger, Neuss, Germany) in 3 female mice with a body-weight between $20-25\,\mathrm{g}$, fixed in a stereotactic frame and under isoflurane anaesthesia (Forene, Abott, Wiesbaden, Germany). $400\,\mathrm{nl}$ of the genetically encoded calcium indicator GCaMP6f (UPenn Vector Core, PA, USA) was injected $-300\,\mu\mathrm{m}$ and $-150\,\mu\mathrm{m}$ below the cortex surface in the area of the visual cortex (V1). After injection, a coverslip (Electron Microscopy Sciences, PA, USA; $5\,\mathrm{mm}$ diameter) was used to seal the craniotomy.

For *in vivo* imaging, the mice were anesthetized with isoflurane to induce persistent and slow wave brain states. In addition, the breathing rate was used as an indicator and monitored to assess the physiological condition of the animals. To induce a persistent brain state, a mixture of isoflurane/oxygen of $0.6-1\,\%$ was used, the breathing rate was $100\,/\,\mathrm{min}$. To induce a slow wave brain state, we used a relation of $1-1.5\,\%$ at a breathing rate of $50-70\,/\,\mathrm{min}$.

Imaging was performed at a two-photon microscope (LaVision Biotech, Bielefeld, Germany) with an excitation wavelength of $920\,\mathrm{nm}$ at $5-20\,\%$ of maximum laser power ($3\,\mathrm{W}$). The focus point was at $200\,\pm\,50\,\mu\mathrm{m}$ with a field of view of $325\times325\,\mu\mathrm{m}$. The sample rate was $30.5\,\mathrm{Hz}$. By that, the optical correlate of neuronal spiking of a local microcircuit comprising about $100-200\,\mathrm{neurons}$ in layer II/III of mouse visual cortex is measured. Here, we integrated the activity of the entire microcircuit.

ISBN 978-90-827970-1-5

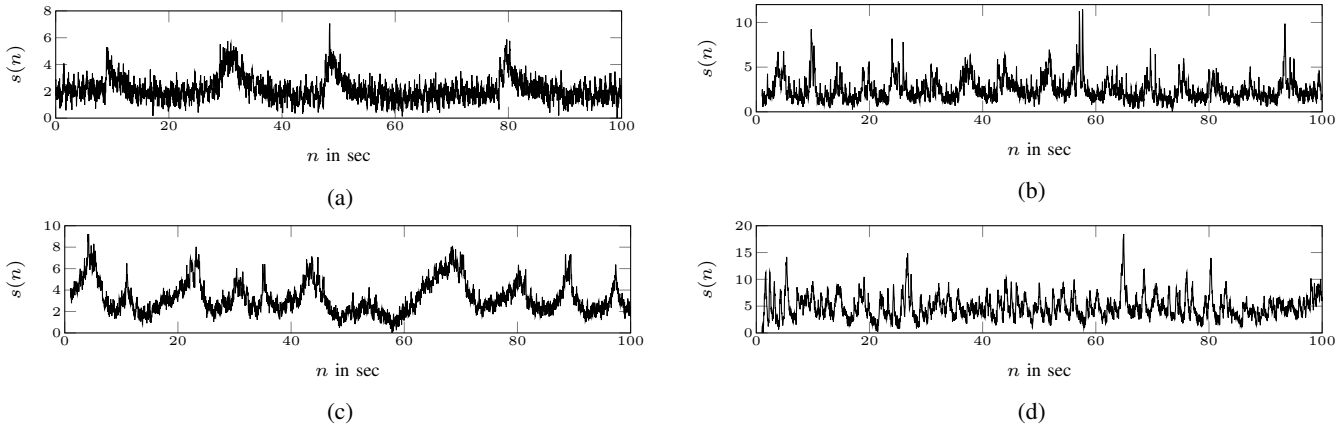

Fig. 1: Examples of signals in slow wave brain state (a)-(c) and in persistent brain state (d).

The remainder of this paper is organized as follows. In Section II, the recorded time series are analyzed first in the time domain and then in the time-frequency domain. Based on their time-frequency representations, several spectral features are extracted, which are used in Section III to formulate a binary hypotheses test to discriminate between the slow wave and the persistent brain states. In Section IV, experimental results based on real data are given. Section V concludes the paper.

II. Characteristics of Slow Wave and persistent brain states

A. Characteristics in the Time Domain

Examples of time series that were observed in different brain states are shown in Fig. 1. Note that the depicted signals have already been detrended using the empirical mode decomposition method [6]. In the persistent brain state, see Fig. 1d, the time series shows rapid and irregular signal fluctuations. In contrast, in Figs. 1a to 1c, it can be seen that the slow wave brain state is associated with Up-Down transitions, consisting of hyperpolarized Down states and intermittent depolarized Up states [1]. The Up state and the Down state correspond to a pulse-shaped transient and a comparatively steady region between the offset and the onset of the transients, respectively. Comparing the three examples for time series in the slow wave brain state leads to two main observations. First, the frequency of occurrence and the duration of the state transients are noticeably different. Unlike the long-lasting Down state in Fig. 1a, the Down states in Fig. 1b and Fig. 1c are difficult to identify. According to the experimental observation, the Up state transients occurred with frequencies ranging from 3 to 10 events per minute, depending on the level of anesthesia. The second observation is that the shapes of the Up state transients differ from subject to subject. In Fig. 1a, the transient has a steep onset and a slowly decaying offset. Clearly, the transients in Fig. 1c have a distinctly different shape. Moreover, the amplitudes of the transients depend on many local parameters, including the level of Ca2+ indicator inside cells and the intensity of the excitation light [1], so that they differ over time and among subjects. In summary, these effects make it difficult to detect slow wave brain states directly in the time domain.

B. Time-Frequency Representations

In order to reveal more characteristics, it is useful to transform the time series to the time-frequency domain. A quadratic time-frequency distribution of a non-stationary signal presents its power distribution over the time-frequency plane. Here, we choose the spectrogram since it provides a good tradeoff between simplicity and performance, i.e., cross-term suppression.

Fig. 2 depicts examples of spectrograms at different states and of different subjects. Figs. 2a to 2c depict the spectrograms of slow wave brain state signals and Fig. 2d depicts the spectrogram of a persistent brain state signal. In the slow wave brain state, there is a high frequency line around 6 to 8 Hz. The intensity of this line, however, varies with subjects. A high frequency line is also present in the persistent brain state, but it differs from the slow wave brain state in that it is located at a higher frequency range, namely, 8 to 10 Hz. However, it is possible that this high frequency component is caused by breathing or other unknown artifacts that are unrelated to the brain activity. Hence, a better understanding of this high frequency component is needed and further experiments will be conducted to explore its origin. In this paper, we show detection results when including and excluding this high frequency component.

In addition to the high frequency line, a low frequency line is present in the slow wave brain state at around 1 Hz. From a neurophysiological perspective, this frequency line is a much more reliable indicator for the slow wave brain state than the high frequency component. It is worth noting that a similar line in the same frequency range is occasionally observed in the persistent brain state as well. This raises the question whether the respective frequency component is present in the persistent brain state as well, or if it is caused by a superposition or alternation of slow wave and persistent brain states.

ISBN 978-90-827970-1-5 © EURASIP 2018

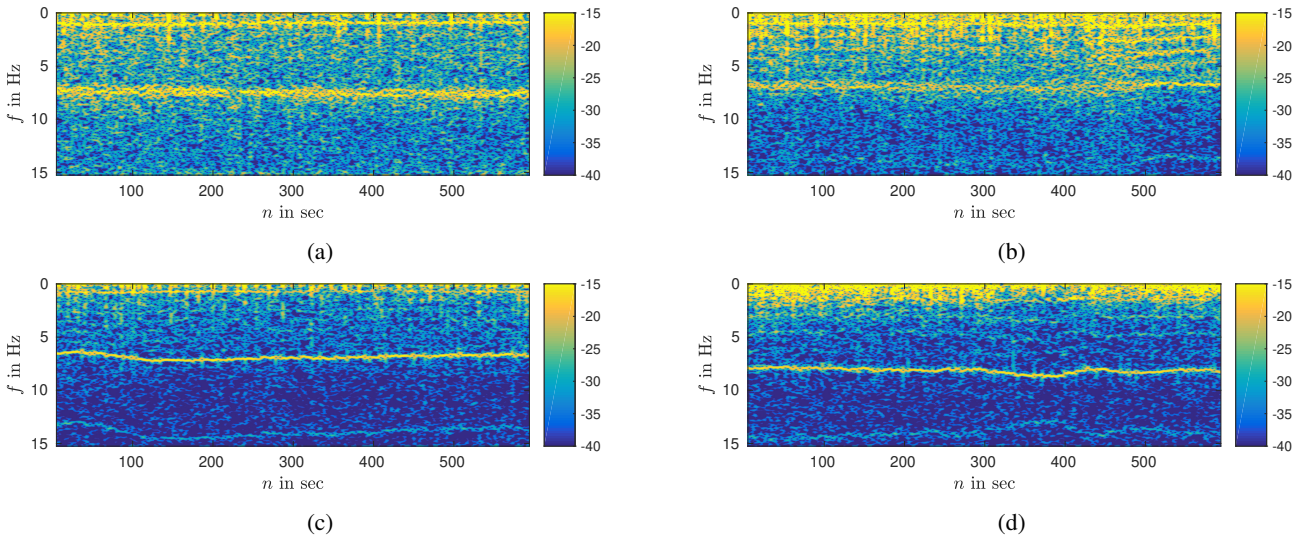

Fig. 2: Examples of spectrograms (Hamming window of 10 seconds) in slow wave brain state (a)-(c) and in persistent brain state (d).

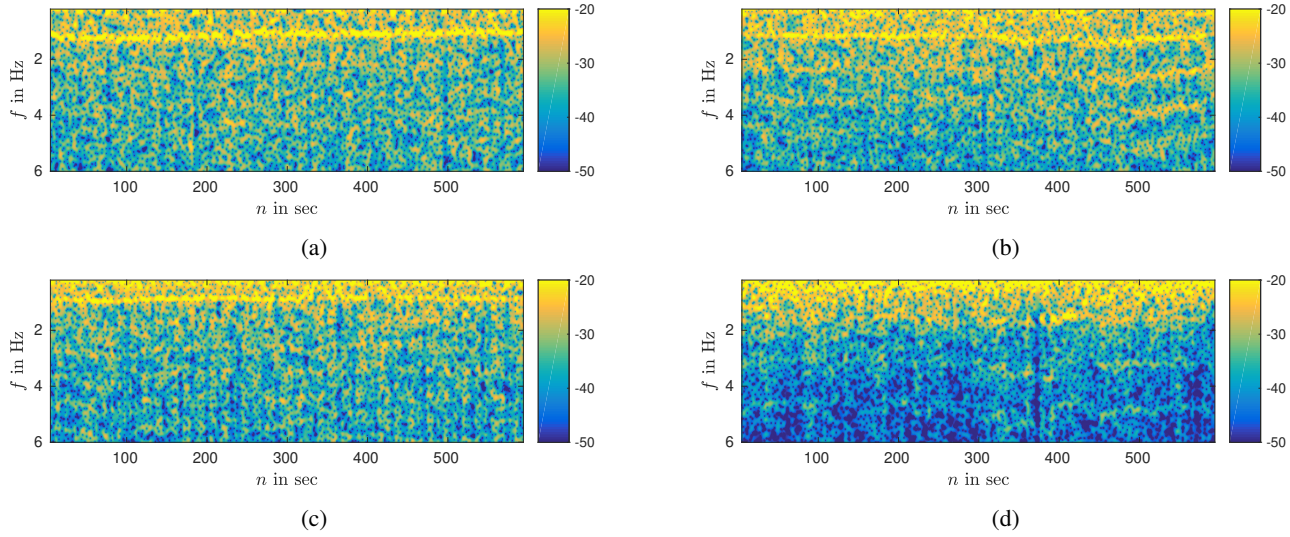

Fig. 3: Examples of normalized spectrograms (Hamming window of 10 seconds) of bandpass filtered signals in slow wave brain state (a)-(c) and in persistent brain state (d).

The spectrogram of the persistent brain state signal is dominated by low frequency components $<2\,\mathrm{Hz}$. In contrast, in the two examples of the slow wave brain state in Figs. 2a and 2b, there is a larger share of power in the frequency region $>2\,\mathrm{Hz}$. The third example in Fig. 2c differs from the previous two examples in that most power is concentrated in a relative narrow low frequency region $<0.2\,\mathrm{Hz}$. The reason is that its corresponding time series, depicted in Fig. 1c, is oscillating at a very low frequency. The amplitude of these slow oscillations is substantially larger than that of the superimposed fast oscillations, leading to dominant low frequency components. Since they obfuscate the relative power distribution among the higher frequencies, the high-power low frequency components are filtered out in order to extract the power percentage feature, see Section III-B.

We conclude this section by stating several minor observations, which are not used in the detection approaches, but are included for completeness. A nonlinear high frequency component at around 13 to $15\,\mathrm{Hz}$ is observed in several examples, both in slow wave and persistent brain states. Furthermore, several examples of both states contain harmonic components. Additionally, repetitive short vertical lines located in low frequency regions are present in several examples in the slow wave brain state, as shown in Figs. 2a and 2c. The temporal positions of these vertical lines correspond to the time instances with rapid variation, for example, during the transition from a Down state to an Up state in Fig. 1a. However, if the Up states occur in rapid succession, as is the case in Fig. 1b, this phenomenon is not visible in the spectrogram – compare Fig. 2b.

ISBN 978-90-827970-1-5

III. State Detection

A. Problem Formulation

We formulate the brain state detection problem as a binary hypothesis test with the two hypotheses, namely

$$\begin{aligned} \mathcal{H}_0: &\quad \text{persistent brain state,} \\ \mathcal{H}_1: &\quad \text{slow wave brain state,} \end{aligned} \tag{1}$$

which are referred to as the null hypothesis and the alternative hypothesis, respectively. The hypothesis test is performed using several features that are calculated for every time instant n and are denoted by $\mathbf{v}(n)$. More details on the features are given in the subsequent section. Finally, the detector $\mathcal{D}$ maps a feature vector $\mathbf{v}(n)$ to a decision d for one of the two hypotheses, i.e.,

$$d = \mathcal{D}\left(\mathbf{v}(n)\right) \in \{0, 1\}, \tag{2}$$

where 0 and 1 represent $\mathcal{H}_0$ and $\mathcal{H}_1$, respectively.

B. Feature Extraction

Several features are extracted from the time-frequency distribution of the time series based on the observations in Section II-B. The spectrogram of the filtered signal is calculated as

$$S(n,k) = \left| \sum_{m=0}^{M-1} s(n-m) w(m) e^{-j2\pi \frac{mk}{M}} \right|^2, \tag{3}$$

where $n = 0, \ldots, N-1$ denotes the time index, $s(\cdot)$ is the time series of length $N \in \mathbb{N}$, $w(\cdot)$ is a window function of length $M \in \mathbb{N}$ and k is the frequency bin index [7].

To extract the frequency line within the interval 6 to 10 Hz, we calculate the frequency corresponding to the highest power density over this region. More specifically, the frequency bin with the highest power, denoted by $k_h(n)$, is defined as

$$k_h(n) = \arg\max_k S(n,k) \quad \text{s.t.} \quad f_h(n) \in [6, 10]\,\text{Hz}, \tag{4}$$

where $f_h(n)$ denotes the physical frequency corresponding to the bin with index $k_h(n)$. In what follows, the one-to-one mapping between the indices and the physical frequencies is denoted by $l(\cdot)$, i.e.,

$$f_h(n) = l(k_h(n)) \quad \text{and} \quad k_h(n) = l^{-1}(f_h(n)). \tag{5}$$

Estimating the frequency line around 1 Hz in real time is challenging since it is occasionally covered by its neighboring low frequency components and its value varies with the experiment subject. To capture this feature, two closely related quantities are considered. The first one aims at approximating the frequency location of the line and, for each time instance n, it is calculated by finding the frequency that corresponds to the dominant peak of $S(n,k)$ within the interval 0.5 to 2 Hz. This frequency is denoted by $f_l(n)$. On the basis that the low frequency line is located between 0.8 Hz and 1.5 Hz in all experimental data, we define the variable $f_l^i(n)$ that indicates whether the low frequency line is located within this frequency band or not, namely

$$f_l^i(n) = \begin{cases} 1, & f_l(n) \in [0.8, 1.5]\,\text{Hz}, \\ 0, & \text{otherwise.} \end{cases} \tag{6}$$

It should be highlighted that the low frequency line can be better identified by considering a longer time series instead of only the current time-frequency distribution $S(n,k)$. However, this comes at the cost of an additional latency. Furthermore, the threshold-values are selected based on the experimental data. Adjusting these values has the potential of improving the detection performance. This, however, is beyond the scope of this paper.

To characterize the differences in the power distribution in both states, the percentage of power in the frequency region $<$2 Hz is considered as an additional spectral feature. To this end, the time series $s(n)$ is first filtered with a bandpass filter with a passband at 0.2 to 6 Hz so that the influence of the high frequency line above 6 Hz and the high-power low frequency component $<$0.2 Hz, which is cause by the slow oscillations, are eliminated. Subsequently, the spectrogram of the bandpass-filtered time series is normalized at each time instance and the percentage of power in the band 0.2 to 2 Hz, denoted as $P_E(n)$, is defined by

$$P_E(n) = \sum_{k=l^{-1}(0.2)}^{k=l^{-1}(2)} S_{\text{BP, norm}}(n,k), \tag{7}$$

where $S_{\text{BP, norm}}(n,k)$ is the normalized spectrogram of the bandpass filtered signal, i.e.,

$$\sum_{k=l^{-1}(0.2)}^{k=l^{-1}(6)} S_{\text{BP, norm}}(n,k) = 1. \tag{8}$$

The normalized spectrograms are depicted in Fig. 3. After normalizing and removing the dominant low frequency component, the difference in the power distributions in both states becomes noticeable. As shown in Fig. 3d, most power is concentrated in the frequency region below 2 Hz in the persistent brain state. In the slow wave brain state, a larger share of the power is distributed in the frequency region between 2 Hz and 6 Hz, see Figs. 3a to 3c. Therefore, $P_E(n)$ is expected to be high when the subject is in the persistent brain state and to be low in the slow wave brain state.

C. Binary Hypothesis Testing Methods

First, a hypothesis test based on each single feature is considered. In this case, a nonparametric threshold test is performed, since the underlying distributions of the features are unknown [8]. Using the percentage of power as an example, i.e., $\mathbf{v}(n) = P_E(n)$, the nonparametric threshold test is defined by

$$d = \begin{cases} 0, & P_E(n) > \tau \\ 1, & \text{otherwise} \end{cases} \tag{9}$$

where τ denotes the threshold.

ISBN 978-90-827970-1-5 © EURASIP 2018

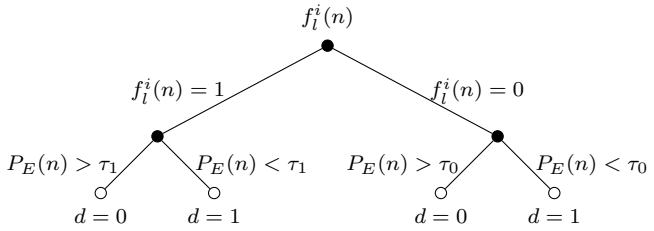

Fig. 4: Decision Tree using $f_l^i(n)$ and $P_E(n)$.

In order to improve the detection performance, we further combined the binary-valued feature $f_l^i(n)$ and the power distribution feature $P_E(n)$. We solve this binary test problem using a decision tree [9]. The decision tree is defined as shown in Fig. 4. In the first step, the value of $f_l^i(n)$ (0 or 1) is calculated to establish whether the slow wave brain state or the persistent brain state is more likely to be true. This splits the test into two branches. In the second step, a nonparametric threshold test is conducted using $P_E(n)$, where the thresholds are τ_1 and τ_0, respectively.

IV. Experimental Results

In order to evaluate the performance of the proposed state detection method, detection is performed at every time instant n and for every test subject. The output of the detector is then compared to manually placed labels that are considered to represent the ground truth.

The detection results based on single features and using the decision tree approach are depicted in Fig. 5. The results are shown in terms of the receiver operating characteristic (ROC), i.e., the detection rate (sensitivity) is plotted against the false alarm rate (specificity). Here, the detection rate represents the probability of correct detection of the slow wave brain state and the false alarm rate represents the probability of erroneous detection. The low frequency component provides the least satisfactory detection result, partially owing to the interruption of the low frequency line, as illustrated in Figs. 3a to 3c. The dashed red line shows the detection result after excluding atypical subjects for which the low frequency component is also observed in the persistent brain state. By inspection, the false alarm rate is significantly reduced for the same detection rate.

The high frequency component $f_h(n)$ provides the best detection performance, followed by the power percentage feature $P_E(n)$. However, as mentioned in the preceding sections, the high frequency component may be associated with artifacts so that it is not clear whether or not it can be considered a characteristic of the brain states. More experiments are required to obtain a better understanding of this frequency line. Surprisingly, a decision tree using both $P_E(n)$ and the low frequency component indicator feature $f_l^i(n)$ achieves results similar to those of the detector based only on $P_E(n)$. This can be explained by the fact that the distributions of $P_E(n)$ are approximately equivalent in both states, i.e. for $f_l^i(n) = 0$ and $f_l^i(n) = 1$. This observation, however, may change as more experimental data become available and as additional features are identified.

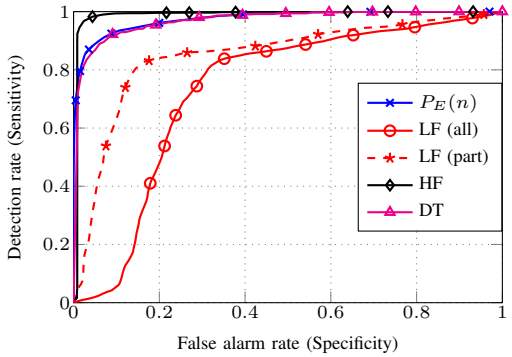

Fig. 5: Detection results in terms of detection rate vs. false alarm rate. HF refers to the high frequency component, DT to decision tree approach, $P_E(n)$ to the percentage of power, and LF (all)/LF (part) denote detection based on the low frequency component including/excluding atypical subject.

V. Conclusion and Outlook

We draw three main conclusions. First, automatically detecting slow wave and persistent brain states seems to be possible with low latency and high accuracy. Considering that even the relatively simple methods proposed in this paper show a reasonable detection performance, we conjecture that focused efforts in this area of research will lead to fast and highly reliable detectors. However, second, further validation is needed with a larger data set. Finally, given more data, a thorough investigation of how to choose a causal and consistent set of features is necessary that also explores signal representations beyond the classic domains of time and frequency.

References

[1] A. Stroh, H. Adelsberger, A. Groh, C. Rhlmann, S. Fischer, A. Schierloh, K. Deisseroth, and A. Konnerth, Making Waves: Initiation and Propagation of Corticothalamic Ca2+ Waves in Vivo, Neuron, 77, pp. 1136–1150, Mar. 2013.

[2] M. Schwalm, F. Schmid, L. Wachsmuth, H. Backhaus, A. Kronfeld, F.A. Jury, P.-H. Prouvot, C. Fois, F. Albers, T.v. Alst, C. Faber, and A. Stroh, Cortex-Wide BOLD fMRI Activity Reflects Locally-Recorded Slow Oscillation-associated Calcium Waves, eLIFE, Sep. 2017.

[3] B. Haider, A. Duque, A.R. Hasenstaub, and D.A. McCormick, Neocortical Network Activity In Vivo Is Generated through a Dynamic Balance of Excitation and Inhibition, J. Neurosci., 26, 4535–4545, Apr. 2006.

[4] L. Gao, X. Meng, C. Ye, H. Zhang, C. Liu, Y. Dan, M.M. Poo, J. He, and X. Zhang, Entrainment of Slow Oscillations of Auditory Thalamic neurons by Repetitive Sound Stimuli, J. Neurosci., 29, 6013–6021, May 2009.

[5] S. Sakata, and K.D: Harris, Laminar Structure of Spontaneous and Sensory-Evoked Population Activity in Auditory Cortex, Neuron, 64, 404–418, Nov. 2009.

[6] N.E. Huang, Z. Shen, S.R. Long, M.C. Wu, H.H. Shih, Q. Zheng, N. Yen, C.C. Tung, and H.H. Liu, The Empirical Mode Decomposition and the Hilbert Spectrum for Nonlinear and Non-stationary Time Series Analysis, Proc. R. Soc. A, 454, March 1998.

[7] L. Stanković, M. Daković and T. Thajyparan, Time-Frequency Signal Analysis with Applications, Artech House, Boston, London, 2013

[8] H.V. Poor, An Introduction to Signal Detection and Estimation, Springer Science & Business Media, 2013

[9] K.P. Murphy, Machine Learing: A Probabilistic Perspective, The MIT Press, 2012

ISBN 978-90-827970-1-5 © EURASIP 2018